ChemComm

Check for updates

Electrochemical lithium-ion insertion/extraction reactions of multilayered graphene with random twist angles†

Satoshi Yamamoto,[a] Ryotaro Sakakibara,[b] Soichi Shima,[a] Shinsuke Matsuura,[a] Takeshi Yajima,[a] Munekazu Motoyama,[ac] Wataru Norimatsu,[bd] Yuta Kimura, [e] Koji Amezawa[e] and Yasutoshi Iriyama [*a]

A multilayer graphene film with random twist angles between layers (TAGr) on SiC($000\bar{1}$) shows six pairs of redox peaks for Li$^+$ insertion/extraction reaction. The distributed twisted angle in TAGr regulates Li$^+$ insertion sites, and smaller *c*-axis expansion (3%) is realized by Li$^+$ insertion.

Graphite is a common anode material for lithium-ion batteries (LIB).[1] Lithium-ion (Li$^+$) insertion reaction into graphite forms five species of stage structure before reaching a maximum Li composition, stage-1 (LiC$_6$). The stages coexist during the Li$^+$ insertion/extraction reactions, and the resultant redox peaks are generally observed at 0.21, 0.12, and 0.085 V.[2] Graphite has ordered AB stacking of graphene (Gr) layers, and the Li$^+$ insertion slides the Gr layers from AB stacking to AA stacking, which recovers to the original AB stacking by Li$^+$ extraction reaction.

On the other hand, soft and hard carbons have received alternative advanced anode materials. These carbons contain "turbostratic structure (TS)", in which Gr layers are well-stacked layer-by-layer with a twisted angle (TA). This twisted stacking restricts the slide formation of AA stacking by Li$^+$ insertion. In addition, these carbons contain pores and poorly stacked structures providing Li$^+$ storage regions.[3–6] Because of these unique structures, for example, hard carbon shows several exciting features compared with graphite, such as higher

capacity,[5] smaller volume change during charge–discharge reactions,[7] reversible Na$^+$ insertion/extraction reactions,[8,9] *etc.* Although there are many works on Li$^+$ storage in soft and hard carbons, the detailed mechanism still remains unclear.[10]

Among the various unique structures of those carbon electrodes, this work aims to understand Li$^+$ insertion/extraction reactions only of the TS region using a model carbon film. Here, we prepared multilayered dense graphene films with random twist angles between layers (TAGr) by thermal decomposition of SiC($000\bar{1}$).[11,12] The TAGr contains a large population of Gr layers rotated at around 30° to SiC, but the TA in the layer-by-layer direction and between in-plane grains is random.[13] Thus, this TAGr will be considered as a model electrode of TS without pores. To detect Li$^+$ insertion/extraction steps into the TAGr, we combined the TAGr with an inorganic Li$^+$ conductive solid electrolyte, lithium phosphorus oxynitride glass electrolyte (LiPON). The TAGr/LiPON combination eliminates the irreversible reductive current by solid electrolyte interphase (SEI) formation commonly observed in LIBs.[13] This combination is helpful in detecting redox peaks by Li$^+$ insertion/extraction reactions of TAGr with high sensitivity.[14]

TAGr was synthesized by thermal decomposition of SiC($000\bar{1}$) substrates.[15] N-doped on-axis 4*H*-SiC wafers with C-terminated ($000\bar{1}$) wafers (CREE research) were cut into 5 mm squares. The substrate was cleaned by ultrasonication in ethanol and acetone. Then, surface oxide layers on SiC were removed with 10 wt% hydrofluoric acid. The resultant chemically polished SiC substrates were heated in an Ar atmosphere (*ca.* 1 atm.) at 1650 °C for 10 min in a furnace. The heating process was carried out as follows: the temperature was raised from room temperature to 800 °C during the initial 2 min and then from 800 °C to 1650 °C during the next 3 min. After keeping the temperature at 1650 °C for 10 min, the cooling process was carried out naturally from 1650 °C to room temperature.

For the fabrication of the Li/LiPON/TAGr/SiC stack (SE-cell), an 8 μm-thick LiPON film was initially deposited onto TAGr by

[a] *Department of Materials Design Innovation Engineering, Nagoya University, Furo-cho, Chikusa-ku, Nagoya, Aichi, 464-8603, Japan.*
E-mail: iriyama.yasutoshi@material.nagoya-u.ac.jp

[b] *Department of Chemical Systems Engineering, Nagoya University, Furo-cho, Chikusa-ku, Nagoya, Aichi, 464-8603, Japan*

[c] *Kyushu University Platform of Inter-Transdisciplinary Energy Research, Kyushu University, Kasuga, Fukuoka, 816-8580, Japan*

[d] *Faculty of Science and Engineering, Waseda University, Tokyo, 169-8555, Japan*

[e] *Institute of Multidisciplinary Research for Advanced Materials, Tohoku University, Katahira, Aoba, Sendai, Miyagi, 980–8579, Japan*

radio frequency (RF) magnetron sputtering in a N_2 atmosphere (4 Pa, 50 W)[16] using a Li_3PO_4 sintered target. Then, Li film was deposited on the LiPON by vacuum evaporation. Each process was carried out without exposing the samples to the air. Cyclic voltammetry (CV) measurements were conducted at 25 °C with a potential sweep rate (v) of 0.5 mV s^{-1}. All the electrochemical measurements were performed using a potentiostat–galvanostat (VMP3, Biologic) at 25 °C in a glove box with a dew point below −80 °C.

The *in situ* X-ray diffraction (XRD) measurements were performed at BL19B2 in SPring-8, Japan. The X-ray energy was 15 keV, and XRD measurements were performed at room temperature. The SE-cell (LiPON thickness was reduced to 2 μm) was sealed in a gas-tight holder in a glove box with a dew point below −70 °C. The X-rays were radiated to the SE-cell through a Kapton dome in the holder. Ar gas was flowed in the holder during the measurements. The voltage of the SE-cell was swept by CV in the charging and discharging directions using a potentiostat–galvanostat (SP-150, Biologic). Before each XRD measurement, the SE-cell was held at a given voltage for 10 minutes.

Fig. 1 shows a cross-sectional transmission electron microscopy (TEM) (JEM2100, JEOL, 200 kV) image of a TAGr. The TEM specimen was prepared by Ar-ion milling after bonding the TAGr with a dummy SiC substrate using epoxy resin.[17] The lattice fringes of the Gr layers are observed parallel to the SiC substrate surface in the magnified image of Fig. 1. The interlayer distance of Gr is estimated to be 0.37 nm from the TEM image. An amorphous layer (*ca.* 2 nm in thickness) composed of Si and C was observed between the SiC substrate and the Gr layers, which will probably be grown during TEM specimen preparation. The average number of Gr layers in TAGr was six as shown in Fig. 1, but some other locations showed more than 20 layers (Fig. S1, ESI†). The variation of the Gr layer numbers depends on multiple nucleation of Gr with different Gr layers on SiC(000$\bar{1}$) and uncontrolled factors in the current stage.[18]

Fig. 2a shows an atomic force microscopy (AFM, SPA-400, SII) image measured by dynamic force mode using a Si-microcantilever (SI-DF20, Hitachi High-Tech Fielding). Several lines in Fig. 2a are wrinkles of Gr generated during the cooling process,[18,19] which are higher than the surrounding areas. The area surrounded by the wrinkles is the Gr layer with atomical
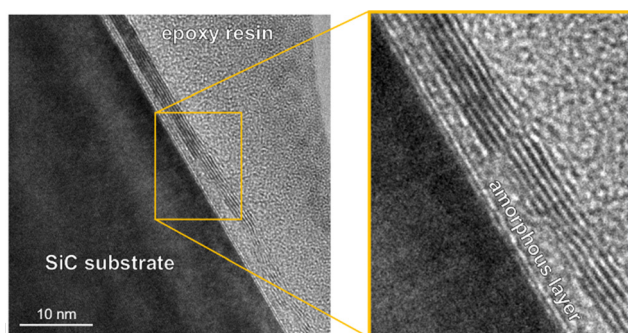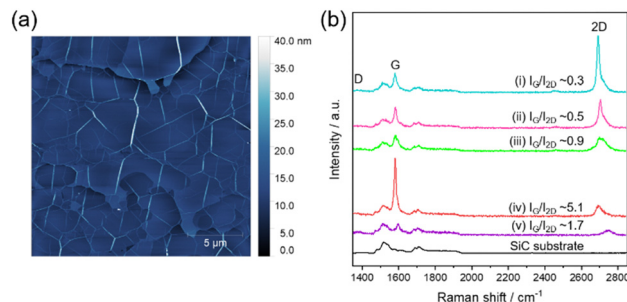

Fig. 2 (a) Topographic AFM image of TAGr grown on a SiC(000$\bar{1}$) substrate. (b) Raman spectra of the TAGr and SiC(000$\bar{1}$) substrate. Each spectrum was measured at different points in the same sample.

flatness. The AFM image shows the height gradient from top to bottom, which is related to the gradient of the SiC (000$\bar{1}$) substrate.

Fig. 2b shows the Raman spectra (inVia Reflex, Renishaw, 532 nm green laser) measured from a ϕ 1 μm area. Spectra (i)–(v) were obtained at different locations in a TAGr, and the spectrum of the SiC substrate is also shown as the reference. At points (i)–(v), three peaks, the D band (1370 cm^{-1}), G band (1600 cm^{-1}), and 2D band (2700 cm^{-1}), were identified in addition to the SiC substrate-derived spectrum, though each D band was too small to be detected in this scale (Fig. S2, ESI†). The intensity ratio of the G band/2D band (I_G/I_{2D}) depended on the measurement points, and the values were 0.3 (i), 0.5 (ii), 0.9 (iii), 5.1 (iv), and 1.7 (v). In previous reports, ARPES and LEEM analyses have shown that a few-layer Gr layer synthesized by the thermal decomposition of SiC (000$\bar{1}$) is composed of Gr layers with random TA, not AB-stacking,[13] although Gr layers rotated around 30° with respect to the SiC substrate were preferentially presented. Carbon material with TS has a varied I_G/I_{2D} ratio depending on the TA of Gr. In the case of 2 layers Gr, I_G/I_{2D} becomes over one at a TA of 12° or less, while the value becomes less than one at a TA of 14° or more.[20] Also, it has been reported that I_G/I_{2D} of both 2–4 layers Gr with a TA of 1° and 2–3 layers Gr with a TA of 9° and 30° are the same as those of 2 layers Gr.[21] It is considered that the difference of I_G/I_{2D} in spectra (i)–(v) reflects the fact that the Gr synthesized in this study has a different TA at each measurement location. In the case of AB-stacking graphite, this I_G/I_{2D} ratio depends on the number of Gr layers, and the values vary 0.3 for one layer, 0.8 for two layers, 1.3 for three layers, 1.7 for four layers, and 2.1 for multilayer.[22–24] Given that the average number of TAGr is 6, the I_G/I_{2D} ratio will be $1.7 < I_G/I_{2D} < 2.1$ if TAGr has AB-stacking, but the I_G/I_{2D} of TAGr varies outside this range. Thus, the spectra (i)–(v) are from Gr with TA. These results indicate that TAGr is composed of Gr with various TA.[13]

Fig. 3a shows the CV curves (3rd cycle, 1.00–0.02 V *vs.* Li/Li$^+$) of the SE-cells using TAGr and multilayer CVD-Gr (MLGr, *ca.* 150 layers) as a reference.[14] Both SE-cells show open circuit voltage (OCV) of almost 0 V due to automatic Li$^+$ insertion into TAGr during the SE-cell assembly in this work. Therefore, an initial voltage sweep curve from OCV to 1.0 V generated irreversible oxidation current probably due to Li stripping
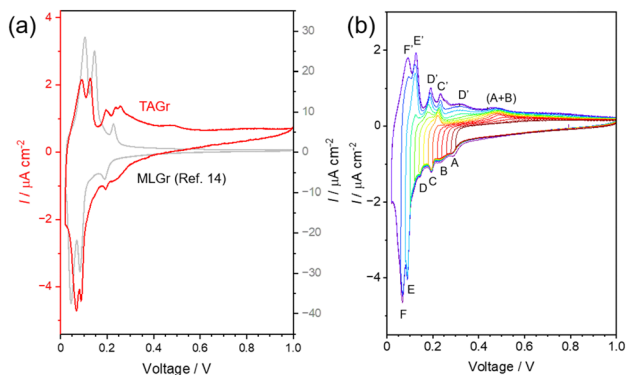

Fig. 1 Cross-sectional TEM image of a TAGr on SiC (000$\bar{1}$).

Fig. 3 (a) The 3rd CV curves of SE-cells using a TAGr (red, left y-axis) and an MLGr (gray, right y-axis (after ref. 14)) at 25 °C. (b) CV curves for a SE-cell using a TAGr. The voltage was swept from 1.00 V to the desired values (0.02, 0.06, 0.08, 0.10, 0.12, 0.14, 0.16, 0.18, 0.20, 0.22, 0.24, 0.26, 0.28, 0.30 V) and then swept to 1.00 V, respectively. $v = 0.5$ mV s^{-1}.

Fig. 4 *In situ* XRD patterns for a SE-cell during (a) charging and (b) discharging. Weaker intensity at 1.00–0.12 V at the charging process is due to beam adjustment to enhance the signal-to-noise ratio. The abscissa is the value of 2θ converted to d-values based on the X-ray wavelength (0.0827 nm). (c) The d-values for voltage during the discharge process.

reaction in addition to Li$^+$ extraction from TAGr. In later cycles, stable CV curves were observed at 0.02–1.00 V (Fig. S3, ESI†).[14] MLGr shows three pairs of redox peaks at 0.21, 0.12, and 0.085 V due to stage transformation during Li$^+$ insertion/ extractions. Both the redox voltages and number of redox peaks are in good agreement with those observed in the dQ/dV curve of graphite.[2] In contrast, TAGr exhibited six couples of redox peaks. This indicates that the Li$^+$ insertion/extraction reactions in TAGr occur through more reaction steps compared with those in MLGr.

To investigate the correspondence of each reductive and oxidative current peak, CVs were measured by stepwise changing the lower potential limit (Fig. 3b). Six reductive current peaks are denoted as A–F from higher voltage to lower voltage. Among these reductive current peaks, the C, E, and F have each corresponding oxidation peaks as C′, E′, and F′, respectively, and the redox peaks that appear resemble voltages with those of MLGr. In contrast, both the A and B correspond to a broad oxidation current (A + B)′, while D has two corresponding oxidation peaks as D′ and D″. Because the SiC/LiPON interface did not show any redox peaks in this voltage range,[25] all the redox peaks will relate with Li$^+$ insertion/extraction reaction to TAGr. Carbon material with TA has been reported to show different numbers of redox peaks compared with that of graphite. For example, in the case of soft carbon, mesocarbon microbeads thermally treated at 2800 °C and 2300 °C have 5 and 4 pairs of redox peaks in the dQ/dV curve, respectively.[26] Also, needle cokes show four oxidation current peaks at slow potential sweep.[27] In the case of hard carbon, the carbon prepared from methylnaphthalene-derived isotropic pitches shows two oxidation current peaks at slow potential sweep.[5] Our dense TAGr exhibited six redox peaks, which is the largest number of redox peaks for Li$^+$ insertion/extraction reactions of carbon material with TA, to the best of our knowledge. Because TAGr is combined with LiPON, its redox reaction peaks will be sensitively detected.[14] In fact, the redox peaks were not distinguished in the CV in a conventional organic liquid electrolyte cell (Fig. S4, ESI†).

In situ synchrotron XRD measurements were performed at several voltages during the charge–discharge process of an SE-cell (Fig. S5a, ESI†). Fig. 4a and b show the XRD patterns measured during the charge (Li$^+$ insertion) and discharge (Li$^+$ extraction) reactions. The intense peaks at $d = 0.336$ nm and $d = 0.505$ nm observed in every pattern are from SiC(0003) and SiC(0002), respectively[28] (Fig. S5b, ESI†). Broad diffraction peaks at $d = 0.34$–0.36 nm correspond to the Gr interlayer of TAGr. Fig. 4c shows the voltage dependence of the d-value of TAGr during the discharge. The d-values tended to decrease from $d = 0.355$ nm to $d = 0.344$ nm with increasing the voltage from 0.02 V to 1.00 V. This trend suggests that the discharge reaction of TAGr proceeds with Li$^+$ extraction from the Gr interlayer. The d-value at 1.00 V for the almost delithiated state (0.344 nm) was consistent with the interlayer distance of carbon with complete TS, and the value is larger than that of graphite (0.335 nm).[29,30] On the other hand, the d-value at 0.02 V (0.355 nm) was smaller than that of stage-1 graphite (0.370 nm).[2] The c-axis expansion of TAGr by intralayer Li$^+$ insertion is estimated to be 3%, which is *ca.* 1/3 of that in graphite (10%).[31] Besides these d-value changes, a broad peak at $d = 0.39$–0.40 nm was observed and disappeared in the intermediate of both at charging (0.12–0.28 V) and discharging (0.22–0.40 V) reactions. This new peak is unique to TAGr and has not been reported in the case of graphite.

The d-value at 0.02 V (0.355 nm) with sufficient Li$^+$ inserted TAGr is smaller than the stage-1 graphite (0.370 nm). Assuming that the Gr interlayer distance with and without Li$^+$ insertion in TAGr is 0.370 nm and 0.344 nm, the average Gr interlayer distance is calculated to be 0.357 nm when both interlayers are alternately stacked as with stage-2 graphite. This value is close to the d-value of TAGr at 0.02 V. Therefore, we can expect that the Li$^+$-inserted region in TAGr is widely dispersed even at a sufficiently Li$^+$-inserted state. TAGr is formed as a stack of Gr layers with random TA. Such twisted Gr layers are known to form superlattices of pseudo-AA stacking islands called moiré patterns.[32,33] The island appears regularly in a given TA, and its radius and distance depend on the TA.[34,35] When the pseudo-AA-stacking region offers Li$^+$ insertion

sites,[35] the Li$^+$-inserted region in-plane will separate much longer than Li$^+$-inserted graphite. This situation may provide gradient regions on d-values between the Li$^+$ inserted site and non-inserted region, generating a slightly wider full-width at half maximum of the X-ray diffraction peak from TAGr at 0.02 V than at 1.00 V. Although the origin of a larger d-value (d = 0.39–0.40 nm) is unclear, poorly stacked layers with longer d-value (>0.37 nm) may be formed during the reactions,[11] though further detailed analyses are required. Although our CV measurements detect six redox peaks, the practical Li$^+$ insertion/extraction reaction of the TAGr will proceed with more reaction steps than graphite. If TAGr is synthesized with uniform TA, the correspondence between the redox peak and the TA will be further clarified, though fabrication of such TAGr is another topic to be addressed in the future.

In summary, multilayered dense graphene films (six Gr layers on average) with random twist angles between layers were prepared as a model electrode of the TS region present in soft and hard carbons, and their Li$^+$ insertion/extraction reactions were investigated combined with LiPON. The TAGr exhibited six redox peaks at 1.0–0.02 V ($vs.$ Li/Li$^+$) in the CV different from MLGr exhibiting three redox peaks. The c-axis expanded by $ca.$ 3% by Li$^+$ insertion, which is lower than that of graphite. In soft and hard carbon electrodes, positive effects of the TS region will be to provide Li$^+$ diffusion pathways and contribute to smaller volume change, while negative effects will be smaller capacity due to limited AA stacking possibly working as Li$^+$ insertion sites. Such positive and negative effects will be important factors for designing those carbon electrodes depending on their applications.

Data availability

The data supporting this article have been included as part of the ESI.†

Conflicts of interest

There are no conflicts to declare.

Notes and references

1 J. M. Tarascon and M. Armand, *Nature*, 2001, **414**, 359–367.
2 T. Ohzuku, Y. Iwakoshi and K. Sawai, *J. Electrochem. Soc.*, 1993, **140**, 2490–2498.
3 M. Winter, J. O. Besenhard, M. E. Spahr and P. Novak, *Adv. Mater.*, 1998, **10**, 725–763.
4 A. Mabuchi, K. Tokumitsu, H. Fujimoto and T. Kasuh, *J. Electrochem. Soc.*, 1995, **142**, 1041–1046.
5 C. W. Park, S. H. Yoon, S. I. Lee and S. M. Oh, *Carbon*, 2000, **38**, 995–1001.
6 H. Azuma, H. Imoto, S. Yamada and K. Sekai, *J. Power Sources*, 1999, **81–82**, 1–7.
7 K. Wang, Y. B. Xu, H. Wu, R. L. Yuan, M. Zong, Y. Li, V. Dravid, W. Ai and J. S. Wu, *Carbon*, 2021, **178**, 443–450.
8 S. Komaba, W. Murata, T. Ishikawa, N. Yabuuchi, T. Ozeki, T. Nakayama, A. Ogata, K. Gotoh and K. Fujiwara, *Adv. Funct. Mater.*, 2011, **21**, 3859–3867.
9 D. A. Stevens and J. R. Dahn, *J. Electrochem. Soc.*, 2000, **147**, 1271–1273.
10 L. J. Xie, C. Tang, Z. H. Bi, M. X. Song, Y. F. Fan, C. Yan, X. M. Li, F. Y. Su, Q. Zhang and C. M. Chen, *Adv. Energy Mater.*, 2021, **11**, 2101650.
11 W. Norimatsu and M. Kusunoki, *J. Phys. D: Appl. Phys.*, 2014, **47**, 094017.
12 Luxmi, N. Srivastava, G. He, R. M. Feenstra and P. J. Fisher, *Phys. Rev. B: Condens. Matter Mater. Phys.*, 2010, **82**, 235406.
13 R. Sakakibara, J. Bao, N. Hayashi, T. Ito, H. Hibino and W. Norimatsu, *J. Phys.: Condens. Matter*, 2023, **35**, 385001.
14 M. Motoyama, K. Miyoshi, S. Yamamoto, R. Sakakibara, Y. Yamamoto, T. Yamamoto, W. Norimatsu and Y. Iriyama, *ACS Appl. Energy Mater.*, 2021, **4**, 10442–10450.
15 K. V. Emtsev, A. Bostwick, K. Horn, J. Jobst, G. L. Kellogg, L. Ley, J. L. McChesney, T. Ohta, S. A. Reshanov, J. Rohrl, E. Rotenberg, A. K. Schmid, D. Waldmann, H. B. Weber and T. Seyller, *Nat. Mater.*, 2009, **8**, 203–207.
16 W. C. West, Y. Ishii, M. Kaneko, M. Motoyama and Y. Iriyama, *ECS Electrochem. Lett.*, 2014, **3**, A99–A101.
17 W. Norimatsu and M. Kusunoki, *Chem. Phys. Lett.*, 2009, **468**, 52–56.
18 W. Norimatsu, J. Takada and M. Kusunoki, *Phys. Rev. B: Condens. Matter Mater. Phys.*, 2011, **84**, 035424.
19 Z. G. Cambaz, G. Yushin, S. Osswald, V. Mochalin and Y. Gogotsi, *Carbon*, 2008, **46**, 841–849.
20 K. Kim, S. Coh, L. Z. Tan, W. Regan, J. M. Yuk, E. Chatterjee, M. F. Crommie, M. L. Cohen, S. G. Louie and A. Zettl, *Phys. Rev. Lett.*, 2012, **108**, 246103.
21 J. Y. Lim, H. S. Jang, H. J. Yoo, S. I. Kim and D. Whang, *Materials*, 2019, **12**, 3740.
22 A. C. Ferrari, J. C. Meyer, V. Scardaci, C. Casiraghi, M. Lazzeri, F. Mauri, S. Piscanec, D. Jiang, K. S. Novoselov, S. Roth and A. K. Geim, *Phys. Rev. Lett.*, 2006, **97**, 187401.
23 Y. Hao, Y. Wang, L. Wang, Z. Ni, Z. Wang, R. Wang, C. K. Koo, Z. Shen and J. T. Thong, *Small*, 2010, **6**, 195–200.
24 Z. Ni, Y. Wang, T. Yu and Z. Shen, *Nano Res.*, 2010, **1**, 273–291.
25 S. Yamamoto, M. Motoyama, M. Suzuki, R. Sakakibara, N. Ishigaki, A. Kumatani, W. Norimatsu and Y. Iriyama, *ACS Nano*, 2023, **17**, 16448–16460.
26 T. Zheng and J. R. Dahn, *Synth. Met.*, 1995, **73**, 1–7.
27 C. W. Park, S. H. Yoon and S. M. Oh, *Carbon*, 2000, **38**, 1261–1269.
28 A. Bauer, J. Krausslich, L. Dressler, P. Kuschnerus, J. Wolf, K. Goetz, P. Kackell, J. Furthmuller and F. Bechstedt, *Phys. Rev. B: Condens. Matter Mater. Phys.*, 1998, **57**, 2647–2650.
29 R. E. Franklin, *Proc. R. Soc. London, Ser. A*, 1951, **209**, 196–218.
30 R. E. Franklin, *Acta Crystallogr.*, 1951, **4**, 253–261.
31 A. Satoh, N. Takami and T. Ohsaki, *Solid State Ionics*, 1995, **80**, 291–298.
32 H. Saadaoui, J. C. Roux, S. Flandrois and B. Nysten, *Carbon*, 1993, **31**, 481–486.
33 M. Endo, K. Oshida, K. Kobori, K. Takeuchi, K. Takahashi and M. S. Dresselhaus, *J. Mater. Res.*, 1995, **10**, 1461–1468.
34 N. N. T. Nam and M. Koshino, *Phys. Rev. B*, 2017, **96**, 075311.
35 D. T. Larson, S. Carr, G. A. Tritsaris and E. Kaxiras, *Phys. Rev. B*, 2020, **101**, 075407.